Temperature- and Pressure-Dependent Kinetics of CH2OO + CH3COCH3 and CH2OO + CH3CHO: Direct Measurements and Theoretical Analysis

Supporting Information

Temperature and Pressure Dependent Kinetics of $CH_2OO + CH_3COCH_3$ and $CH_2OO + CH_3CHO$: Direct Measurements and Theoretical Analysis

Rehab M. I. Elsamra,[†,‡] Amrit Jalan,[†] Zachary J. Buras,[†] Joshua E. Middaugh,[†] and William H. Green.[†*]

[†] Department of Chemical Engineering, Massachusetts Institute of Technology, 77 Massachusetts Avenue, Cambridge, MA 02139, USA.
[‡] Department of Chemistry, Faculty of Science, Alexandria University, Ibrahimia, 21321, Alexandria, Egypt.

UV Absorption experiments at different T and P:

Table S1 summarizes the conditions of the $CH_2OO + CH_3COCH_3/CH_3CHO$ experiments. In all our experiments $[O_2]$ was kept constant (6.1×10^{16} molecule cm^{-3}), $[CH_3COCH_3]$ was varied from $1.59 \times 10^{14} – 1.35 \times 10^{15}$ molecule cm^{-3} and $[CH_3CHO]$ was varied from $1.59 \times 10^{14} – 1.11 \times 10^{15}$ molecule $cm^{-3.}$ The number of flashes per refresh was 1.21 and the photolysis beam diameter = 1.15 cm.

Table S1: Experimental conditions for *T*- and *P*- dependence UV absorbance experiments

Base case experiments	*T* K	*P* Torr	$[CH_2I_2]^a$ molecule/cm^3	Photolysis power mJ/ pulse
T-dependence	(298 ± 1.3) to (494 ± 5)	25	1.35×10^{14}	50
P- dependence	(298 ± 1.3) and (444 ± 3)	4 - 50	1.35×10^{14}	50
Control experiments				
Max. Photolysis energy	(298 ± 1.3) and (494 ± 5)	25	1.35×10^{14}	100
double $[CH_2I_2]$	(298 ± 1.3) and (494 ± 5)	25	2.44×10^{14}	50

[a] $[CH_2I_2]$ was estimated by using the vapor pressure of CH_2I_2 at 298 K[1]

Two absorbance-control experiments were conducted at 298 and 494 K at constant pressure of 25 Torr, one with double the base case precursor concentration ([CH_2I_2]) and the other at maximum photolysis energy (100mJ/pulse). These control experiments were performed to confirm that no interfering secondary chemistry was being observed under the base case conditions. Traces were also recorded in the absence of O_2 or CH_2I_2 at every temperature to ensure that no CH_2OO radicals are formed except under the normal reactor conditions (i.e., with both CH_2I_2 and O_2 gases present) and/or that no other species are contributing to the 375 nm absorbance signal. Results of control experiments are shown in Fig. S1.

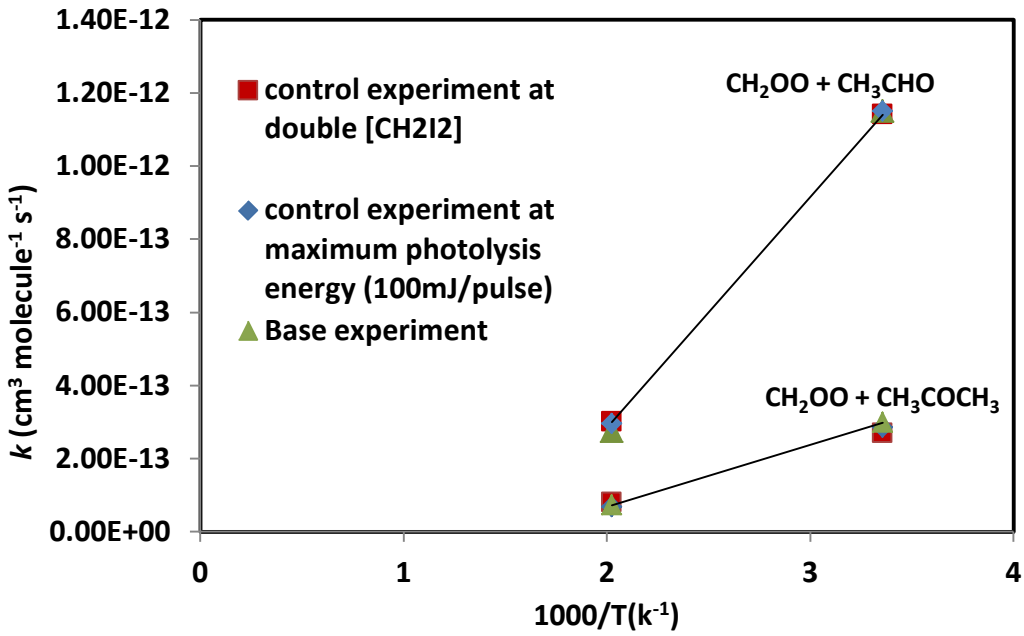

Figure S1. Control experiments at 298 K and 494 K together with the base experiments for CH_2OO + CH_3CHO (top points) and CH_2OO + CH_3COCH_3 (bottom points).

Figure S1 shows example of the control experiments carried out at the double concentration of CH_2I_2 and at maximum laser photolysis energy. As seen in the figure, the control results are consistent with the base condition ([CH_2I_2] = 1.35×10^{14} molecules cm^{-3} and 50 mJ/pulse), implying that the effect of laser energy and precursor concentration on the measured rate coefficients is negligible.

CH_2OO + CH_3COCH_3 MS Control Experiments

In addition to $\frac{m}{z} = 46$ amu (the mass of the simplest CI, CH_2OO), we observed four other transient species in our $\frac{m}{z}$ range of interest (0-104 amu) in the "Base Case" mass spectrometry (MS) experiment: $\frac{m}{z} = 31, 73, 89$ and 104 amu. Transient behavior was not discernible at $\frac{m}{z} = 15$ due to overlap with a CH_3COCH_3 fragment. This Base Case refers to the conditions where CH_2OO + CH_3COCH_3 is occurring and there is also calibration mixture (cal mix) present in the reactor to act as an internal standard (Base Case = CH_2I_2 + O_2 + CH_3COCH_3 + cal mix + 355 nm photolysis). Control MS experiments were conducted without CH_3COCH_3, without O_2 and without cal mix to identify which of these transient species are possible products of CH_2OO + CH_3COCH_3. The maximum signal of transient species i, $S_{i,max}$, was normalized by the initial amount of CH_2I present, $[\mathrm{CH_2I}]_0$ (obtained from simultaneously recorded I Atom Absorbance), and the average internal standard (benzene) signal during that experiment, $\bar{S}_{benzene}$:

$$\hat{S}_{i,max} = S_{i,max}/([\mathrm{CH_2I}]_0 \bar{S}_{benzene})$$

Performing this normalization removes the effect of varying CH_2I concentration and MS signal response from experiment to experiment. The ratio of $\hat{S}_{i,max}$, for a given control experiment with the base case experiment was then taken:

$$\frac{\left(\hat{S}_{i,max}\right)_{Control}}{\left(\hat{S}_{i,max}\right)_{Base\ Case}} = \frac{[i]_{max,Control}}{[i]_{max,Base\ Case}}$$

As shown, this ratio is indicative of how much the concentration of transient species, i, changed going from the Base Case to the control experiment. Table S2 summarizes the results of this analysis for the three control experiments mentioned above. Note that for the "No Cal Mix" control, $\bar{S}_{benzene} = 0$, so for this experiment we had no internal standard to use and we assumed that the signal response of the MS was the same for this control experiment as for the base case. We believe this is a good assumption because the Base Case and "No Cal Mix" experiments were done back-to-back for this reason, and because the Cal Mix was present in such low concentration ($\sim 10^{11}$ molecules cm^{-3} compared to $\sim 10^{17}$ molecules cm^{-3} total at the pressure of these experiments, 10 Torr) that the MS signal response should not be affected by removing it anyway.

Table S2. Results of MS control experiments for CH_2OO + CH_3COCH_3. $\boldsymbol{T = 298\ K}$ and $\boldsymbol{P = 10\ Torr}$. For Base Case experiment: [CH_3COCH_3]= 1.24×10^{15} molecule cm^{-3}, [CH_2I_2] = 2.44×10^{14}, [O_2] = 6×10^{16} molecule cm^{-3} and [Cal Mix Species] = 1.6×10^{11} molecule cm^{-3}. Each Control experiment was conducted under identical conditions as the Base Case experiment, except for the one change noted.

	$\frac{[i]_{max,control}}{[i]_{max,Base\ Case}}$ for $\frac{m}{z}$ =			
MS Control Experiment	31 amu	73 amu	89 amu	104 amu
No Acetone	1.0 ± 0.4	1.3 ± 0.5	0	0
No O_2	1.1 ± 0.4	1.1 ± 0.4	0	0
No Cal Mix.	0.17 ± 0.06	1.7 ± 0.6	1.0 ± 0.4	1.1 ± 0.7

There are several important things to note about these results. First, the species at $\frac{m}{z} = 89$ and 104 amu only appear when both acetone and O_2 are present and their maximum concentrations are not affected by the presence of Cal Mix. Therefore, we conclude that these two species are products of CH_2OO + CH_3COCH_3, consistent with what Taatjes et al. have observed.[2] Second, the species at $\frac{m}{z} = 31$ and 73 amu are present at the same maximum concentration regardless of whether acetone or O_2 are present. Therefore $\frac{m}{z} = 31$ and 73 amu cannot be products of CH_2OO + CH_3COCH_3. Finally, the maximum concentration of $\frac{m}{z} = 31$ decreases substantially without Cal Mix present, indicating that how much $\frac{m}{z} = 31$ is being formed depends on one of the Cal Mix species being present. At the same time that the maximum concentration of $\frac{m}{z} = 31$ decreases with no Cal Mix, the maximum concentration of $\frac{m}{z} = 73$ increases, likely because whatever channels are producing $\frac{m}{z} = 31$ and $\frac{m}{z} = 73$ amu are competing for CH_2I. Therefore, if the rate for the $\frac{m}{z} = 31$ producing channel decrease, there is more CH_2I available to form $\frac{m}{z} = 73$ amu. We think that $\frac{m}{z} = 73$ is produced by a side reaction involving a contaminant in our reactor, which previous to the current Criegee Intermediate studies has been used for studies on the vinyl and allyl radical.

Quantifying Pressure-Dependent Product Yields for CH_2OO + CH_3COCH_3

The kinetic model from the main text is reproduced here for reference.

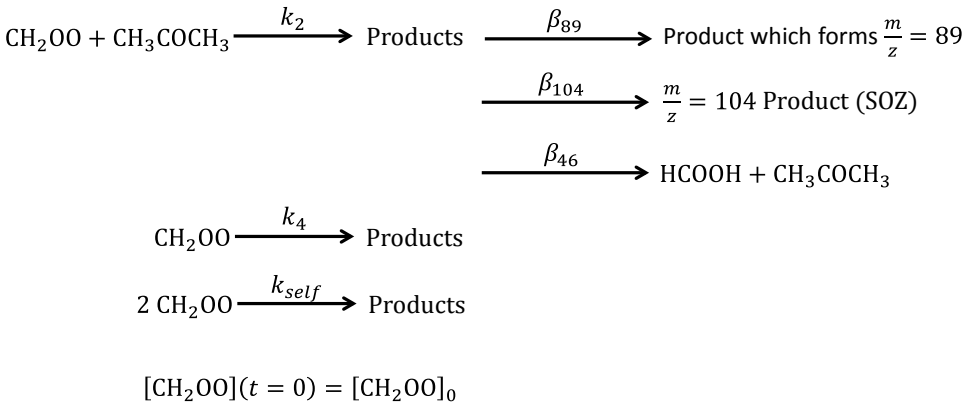

Scheme 1. General kinetic model for CH_2OO + CH_3COCH_3

Assuming that CH_3COCH_3 is present in excess, the analytical expressions for $[CH_2OO](t)$ and the steady state concentration of the CH_2OO + Acetone products, $[Products]_{CI+Acetone}\ (t \to \infty)$, based on the kinetic model above are the following:

$$[CH_2OO](t) = \frac{(k_2[CH_3COCH_3]+k_4)[CH_2OO]_0}{(k_2[CH_3COCH_3]+k_4+2k_{self}[CH_2OO]_0)e^{(k_2[CH_3COCH_3]+k_4)t}-2k_{self}[CH_2OO]_0}$$

$$[\text{Products}_{(CI+Acetone)}](t \to \infty) = \frac{k_2[CH_3COCH_3]}{2k_{self}} \ln\left(\frac{k_2[CH_3COCH_3]+k_4+2k_{self}[CH_2OO]_0}{k_2[CH_3COCH_3]+k_4}\right)$$

It is clear that the time dependence of CH_2OO and the steady state concentration of the products of its reaction with CH_3COCH_3 depend on many parameters: $[CH_2OO]_0$, k_2, k_{self} and k_4. k_2 is known from the UV absorbance experiments also reported in this work. The experiments to quantify the other parameters are discussed below.

The initial concentration of CH_2OO, $[CH_2OO]_0$, in the above equation can be quantified from transient I atom absorbance assuming that $[CH_2I]_0 = [I]_0$. A narrow linewidth low-noise continuous-wave diode laser was used to generate an infrared beam tuned to the ($F = 3\ ^2P_{1/2} \leftarrow F = 4\ ^2P_{3/2}$) I atom atomic transition.[3] The infrared path lengths for I atom absorption were in the range of $50 - 70$ cm. Both ultraviolet

and single-pass infrared absorbance traces were averaged over 500 acquisitions and recorded simultaneously.

We have previously shown that the I atom absorbance, A_I, may be fit adequately to the following equations.[4]

$$[\mathrm{I}](t) = \frac{[\mathrm{CH_2I}]_0}{k_1[\mathrm{O_2}] - k_5}\left([(1+\alpha)k_1[\mathrm{O_2}] - k_5]e^{-k_5 t} - \alpha k_1[\mathrm{O_2}]e^{-k_1[\mathrm{O_2}]t}\right)$$

$$A_I(t) = \sigma_{\mathrm{I}}(\lambda = 1315.246\ \mathrm{nm})\, l_I [\mathrm{I}](t)$$

Where α is the branching fraction of $CH_2I + O_2$ to CH_2OO, k_1 is the total rate of that reaction, k_5 is the first order loss rate of I atom due to various processes, $\sigma_I(\lambda)$ is the known absorption cross section of I atom for a given hyperfine transition and l_I is the measured path length of the I atom laser. In these equations, α and k_1 are global fit parameters and k_5 and $[\mathrm{CH_2I}]_0$ are local fit parameter (i.e. a different value of each is fit for every trace). The quantity $\alpha[\mathrm{CH_2I}]_0$ is equal to $[\mathrm{CH_2OO}]_0$. A representative fit to an I atom trace is shown in Fig. S2.

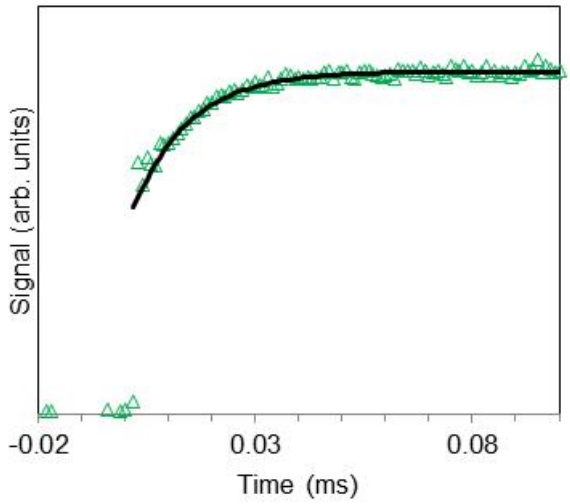

Figure S2. Representative I atom trace at 298 K, 10 Torr and $[\mathbf{O_2}] = \mathbf{6.0 \times 10^{16}\ cm^{-3}}$ with model fit to extract value of $[\mathbf{CH_2OO}]_\mathbf{0}$. Only every 100th point is shown.

The growth in I Atom absorbance shown in Fig. S2, A_I, corresponds to the sum of the initial photolytic production of I, and the production of I by the reaction $\mathrm{CH_2I + O_2 \rightarrow CH_2OO + I}$ with rate $k_1 (= 1.4 \pm 0.1 \times 10^{-12}\ \mathrm{cm^3\ molecule^{-1}\ s^{-1}})$.[4,5] The amount of I Atom produced by the second process, $[\mathrm{I}]_0$, can be captured and is equal to the amount of $[\mathrm{CH_2OO}]$ formed.

The equation for $[Products]_{Cl+Acetone}$ $(t \to \infty)$, also depends on k_{self} and k_4. Until recently, k_{self} had not previously been experimentally measured, although Vereecken et al.[6] had predicted a value of $k_{self} \approx 3.8 \times 10^{-11}\text{cm}^3\text{molecule}^{-1}\text{cm}^{-1}$ using quantum calculations and TST. Very recently and just prior to the current work, our group was successfully able to experimentally measure k_{self} using UV absorption.[7] We measured $k_{self} = 6.2 \pm 2.2 \times 10^{-11}\text{cm}^3\text{molecule}^{-1}\text{cm}^{-1}$, in good agreement with Vereecken et al. and later experimental measurements by Ting et al.[8] and Chhantyal-Pun et al.[9] We used this value of k_{self} in all calculations here.

The value of k_4, which includes diffusion out of the sampling volume, could change significantly if the experimental apparatus is modified. This study was conducted over the course of a few days, however, during which time the reactor was kept as static as possible. Therefore, for a given pressure and temperature, we expect this value to be roughly the same for all of the results reported here.

In order to obtain values for k_4 at 10, 25 and 50 Torr (temperature is always 298 K), the decay of $\frac{m}{z} = 46$ measured by TOF-MS, $S_{46}(t)$, was recorded under conditions where CH_2OO is formed (ie, CH_2I_2 + O_2 + 355 nm photolysis) both with and without CH_3COCH_3. $S_{46}(t)$ was then normalized and fit to the expression for $\frac{[\text{CH}_2\text{OO}](t)}{[\text{CH}_2\text{OO}]_0}$ above. k_4 was used as fit parameter for traces taken at the same pressure while k_2 and k_{self} were fixed to the values measured with UV absorbance earlier. Representative fits to normalized $S_{46}(t)$ with and without acetone and the fitted values obtained for k_4 are given in Fig. S3 and Table S3, respectively.

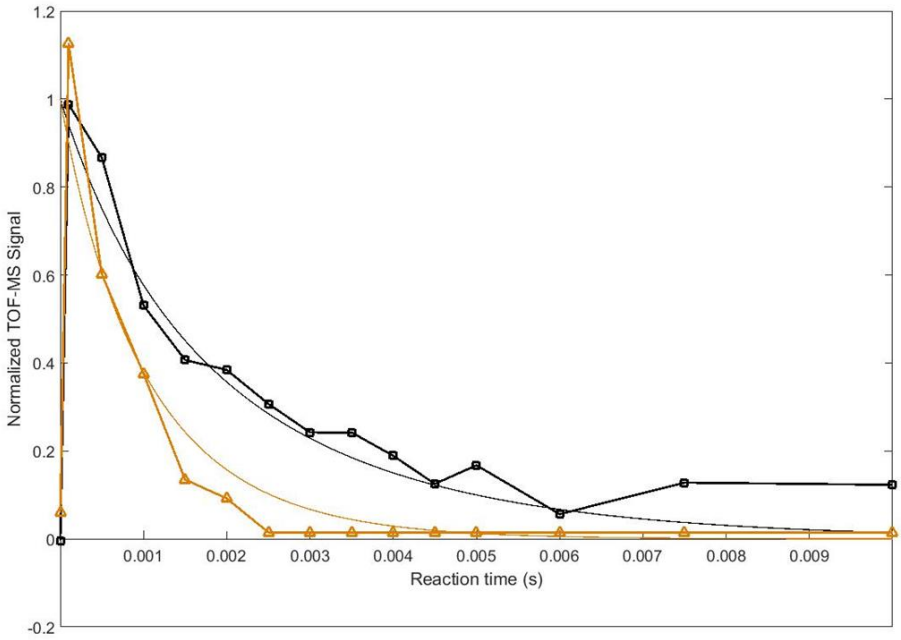

Figure S3. Representative normalized decay of $\frac{m}{z} = \mathbf{46}$ measured by TOF-MS at 298 K, 50 Torr, $[\mathbf{O_2}] = \mathbf{6.0 \times 10^{16} cm^{-3}}$ and $[\mathbf{CH_3COCH_3}] = \mathbf{0}$ (black squares) and $\mathbf{1.24 \times 10^{15}\ cm^{-3}}$ (orange triangles). Thin lines are fits to the kinetic model given in Scheme 1.

Table S3. Values obtained for $\boldsymbol{k_4}$ at 298 K and different pressures.

Pressure (Torr)	$\boldsymbol{k_4}$(s^{-1})
10	**230**
25	**470**
50	**320**

With values of k_2, k_{self} and k_4 known at 10, 25 and 50 Torr, it is possible to calculate $[\mathrm{Products_{CI+Acetone}}](t \to \infty)$ at those conditions for a given $[CH_2OO]_0$ and $[CH_3COCH_3]$.

The steady state concentrations of the $\frac{m}{z} = 89$ and 104 amu product species are related to $[\mathrm{Products_{(CI+Acetone)}}](t \to \infty)$ through their respective branching fractions, β_i, by the following equations.

$$\left[\frac{m}{z} = 89 \text{ amu}\right](t \to \infty) = \beta_{89}\left[\text{ Products}_{(\text{CI+Acetone})}\right](t \to \infty)$$

$$\left[\frac{m}{z} = 104 \text{ amu}\right](t \to \infty) = \beta_{104}[\text{Products}_{\text{CI+Acetone }}](t \to \infty)$$

The general relationship between the PI TOF-MS signal due to a species i, S_i, (measured as integrated peak area) and its concentration is the following.

$$S_i = FR_i\sigma_i(E)[i]$$

Where F is the instrument response factor, R_i is the mass discrimination factor and $\sigma_i(E)$ is the photoionization cross-section of species i at energy E. Accordingly, the steady-state PI TOF-MS signals for $\frac{m}{z} = 89$ amu and $\frac{m}{z} = 104$ amu can be expressed as follows.

$$S_{89}(t \to \infty) = FR_{89}\sigma_{89}(E = 10.5 \text{ eV})\left[\frac{m}{z} = 89 \text{ amu}\right] \quad (t \to \infty)$$

$$S_{104}(t \to \infty) = FR_{104}\sigma_{104}(E = 10.5 \text{ eV})\left[\frac{m}{z} = 104 \text{ amu}\right] \quad (t \to \infty)$$

Or

$$S_{89}(t \to \infty) = FR_{89}\sigma_{89}(E = 10.5 \text{ eV})\beta_{89}\left[\text{Products}_{(\text{CI+Acetone })}\right](t \to \infty)$$

$$S_{104}(t \to \infty) = FR_{104}\sigma_{104}(E = 10.5 \text{ eV})\beta_{104}\left[\text{Products}_{(\text{CI+Acetone })}\right](t \to \infty)$$

In all of our PI TOF-MS experiments, a small amount of a gas mixture with known composition was simultaneously flowed in the reactor to act as an internal standard. The concentrations of calibration mixture species are small so as not to interfere with the chemistry (10^{11} cm^{-3}) and known to within 15% based on the reactor conditions. The mixture contains 101 ppm of each of the following species: methylamine (31 amu), propene (42 amu), 1,3-butadiene (54 amu), propanol (60 amu), furan (68 amu), benzene (78 amu), cyclohexane (84 amu), toluene (92 amu) and heptane (100 amu).

Taking the ratio of $S_{89}(t \to \infty)$ or $S_{104}(t \to \infty)$, to the average PI TOF-MS signal from any of the calibration mixture species, $\bar{S}_{calmix,j}$, results in the following.

$$\frac{S_{89}(t \to \infty)}{\bar{S}_{calmix,j}} = \frac{FR_{89}\sigma_{89}(E = 10.5 \text{ eV})\beta_{89}\left[\text{Products}_{(\text{CI+Acetone })}\right](t \to \infty)}{FR_{calmix,j}\sigma_{calmix,j}(E = 10.5 \text{ eV})[calmix,j]}$$

$$\frac{S_{104}(t \to \infty)}{\bar{S}_{calmix,j}} = \frac{FR_{104}\sigma_{104}(E = 10.5 \text{ eV})\beta_{104}\left[\text{Products}_{(\text{CI+Acetone })}\right](t \to \infty)}{FR_{calmix,j}\sigma_{calmix,j}(E = 10.5 \text{ eV})[calmix,j]}$$

F cancels out because it is a constant. For our apparatus we have found the mass discrimination factor to have very weak or no dependence on mass. Therefore the ratio of R values also becomes one.

$$\frac{S_{89}(t\to\infty)}{\bar{S}_{calmix,j}} = \beta_{89}\frac{\sigma_{89}(E=10.5\text{ eV})}{\sigma_{calmix,j}(E=10.5\text{ eV})}\frac{[\text{Products}_{(\text{CI+Acetone})}](t\to\infty)}{[calmix,j]}$$

$$\frac{S_{104}(t\to\infty)}{\bar{S}_{calmix,j}} = \beta_{104}\frac{\sigma_{104}(E=10.5\text{ eV})}{\sigma_{calmix,j}(E=10.5\text{ eV})}\frac{[\text{Products}_{(\text{CI+Acetone})}](t\to\infty)}{[calmix,j]}$$

These equations can be rearranged for, $\sigma_{89}\beta_{89}$ and $\sigma_{104}\beta_{104}$.

$$\sigma_{89}\beta_{89} = \sigma_{calmix,j}(E=10.5\text{ eV})\frac{S_{89}(t\to\infty)}{\bar{S}_{calmix,j}}\frac{[calmix,i]}{[\text{Products}_{(\text{CI+Acetone})}](t\to\infty)}$$

$$\sigma_{104}\beta_{104} = \sigma_{calmix,j}(E=10.5\text{ eV})\frac{S_{104}(t\to\infty)}{\bar{S}_{calmix,j}}\frac{[calmix,i]}{[\text{Products}_{(\text{CI+Acetone})}](t\to\infty)}$$

The quantity $\sigma_i\beta_i$, where $i = 89$ or 104, cannot be separated because σ_i is not known. If, however, we assume that σ_i is independent of pressure, then we can ratio the measured value of $\sigma_i\beta_i$ at one pressure, $(\sigma_i\beta_i)_{\text{P1}}$, to another pressure, $(\sigma_i\beta_i)_{\text{P2}}$ and cancel out the σ_i values.

$$\frac{(\sigma_i\beta_i)_{\text{P1}}}{(\sigma_i\beta_i)_{\text{P2}}} = \frac{(\beta_i)_{\text{P1}}}{(\beta_i)_{\text{P2}}}$$

Furthermore, if we assume that $\sigma_{calmix,j}$ and σ_i are pressure independent:

$$\frac{(\beta_i)_{\text{P1}}}{(\beta_i)_{\text{P2}}} = \frac{\left(\frac{S_i(t\to\infty)}{\bar{S}_{calmix,i}}\frac{[calmix,i]}{[\text{Products}_{(\text{CI+Acetone})}](t\to\infty)}\right)_{\text{P1}}}{\left(\frac{S_i(t\to\infty)}{\bar{S}_{calmix,i}}\frac{[calmix,i]}{[\text{Products}_{(\text{CI+Acetone})}](t\to\infty)}\right)_{\text{P2}}}$$

This equation was given in the main text. In this manner, the relative pressure dependent yield of both $\frac{m}{z} = 89$ and $\frac{m}{z} = 104$ can be computed.

Note that, of the nine species present in the calibration mix, only benzene is a suitable internal standard. Of the other eight, propene and 1,3-butadiene overlap with acetone fragment signals in the mass spectrum, methylamine and propanol are not thermally stable, furan and heptane have low signal (relatively small cross sections), and the

concentrations of toluene and cyclohexane have decreased below 101 ppm over the lifetime of the gas cylinder. The stable benzene signal used as an internal standard is shown in Fig. S4.

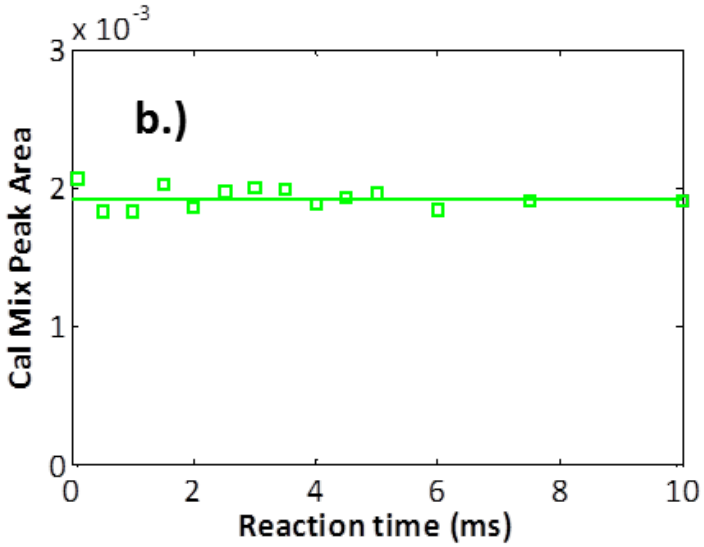

Figure S4. TOF-MS signal of the internal benzene standard at 298 K, 10 Torr, $[\mathbf{O_2}] = \mathbf{5.95 \times 10^{16} cm^{-3}}$ and $[\mathbf{CH_3COCH_3}] = \mathbf{1.24 \times 10^{15} cm^{-3}}$ recorded simultaneously as the product signals shown in Fig. 6. The line is an average values of the stable benzene signal, $\overline{S}_{calmix,benzene}$.

Figure S5 shows the measured values of $\frac{(\beta_i)_{P1}}{(\beta_i)_{P2}}$ for $\frac{m}{z} = 104$ amu as a function of pressure. The TOF-MS signal for this species was too low to discern a trend with respect to pressure (S_{104} has low signal/noise ratio).

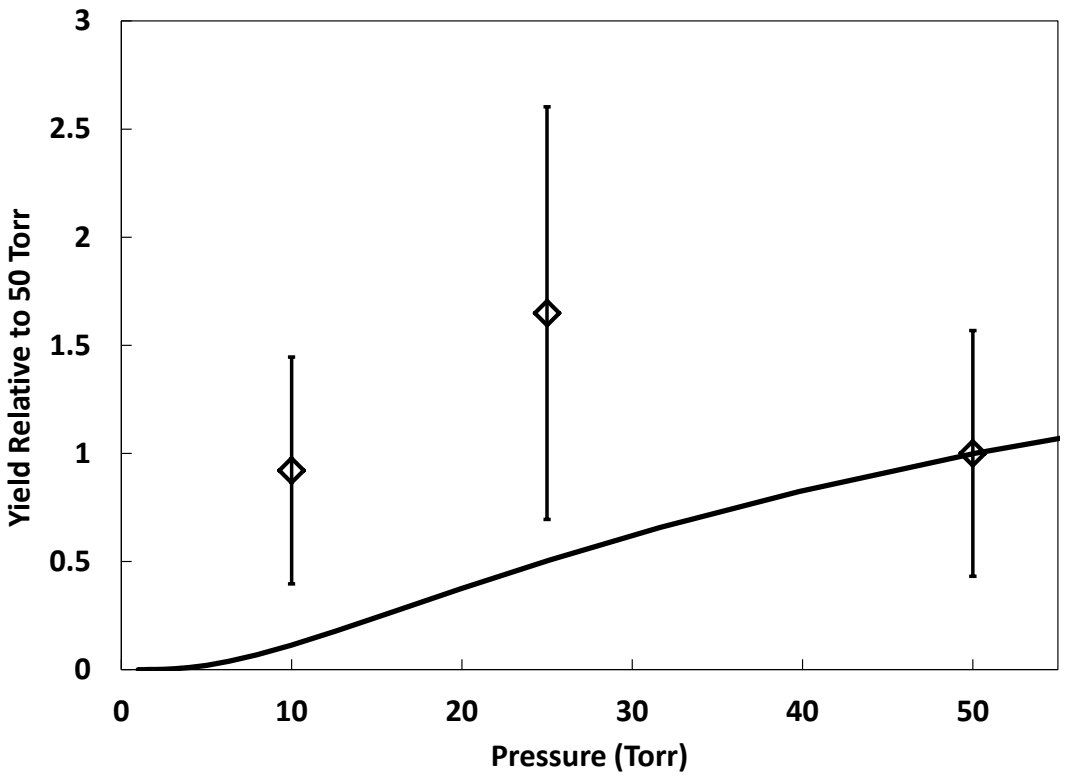

Figure S5. Relative yield of $\frac{m}{z} = 104$ amu product from CH_2OO + CH_3COCH_3 normalized to the 50 Torr measurement $\left(\frac{(\beta_{104})_{\mathrm{P=X\ Torr}}}{(\beta_{104})_{\mathrm{P=50\ Torr}}}\right)$ at 298 K (markers) compared to predicted relative yield of SOZ at the same conditions from Jalan et al.[10] (line). The error bar on the 50 torr point indicates the uncertainty in that measurement (which is used to normalize the other two points.)

Theoretical Calculations

Fig. S6 shows the lack of sensitivity to $k_{outer}^{P=\infty}$ exhibited by $k_{observable}^{P=0}$ and $k_{observable}^{P=\infty}$. Fig. S7 shows the logarithm of the various contributions to the ratio of inner TS to reactant partition functions, $\frac{Q_{TS,inner}}{Q_{reactants}}$, in the expression for $k_{TST}(T)$ below:

$$k_{TST}(\mathrm{T}) = \frac{k_B T}{h}\left(\frac{Q_{TS,inner}}{Q_{reactants}}\right) \times \exp\left(-\frac{\left[E_0^{TS,inner} - E_0^{reactants}\right]}{RT}\right)$$

$$\log_{10}\left(\frac{Q_{TS,inner}}{Q_{reactants}}\right) = \log_{10}\left(\frac{Q_{TS,inner}}{Q_{reactants}}\right)_{rot} + \log_{10}\left(\frac{Q_{TS,inner}}{Q_{reactants}}\right)_{vib} + \log_{10}\left(\frac{Q_{TS,inner}}{Q_{reactants}}\right)_{trans} + \log_{10}\left(\frac{Q_{TS,inner}}{Q_{reactants}}\right)_{hindered\ rotor} + \log_{10}\left(\frac{Q_{TS,inner}}{Q_{reactants}}\right)_{optical\ isomers}$$

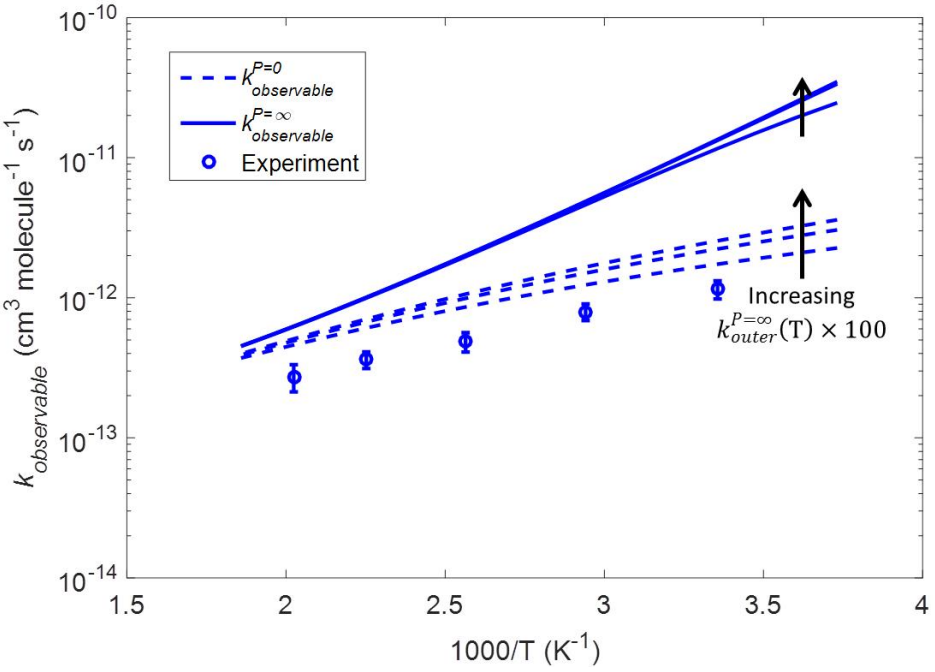

(a)

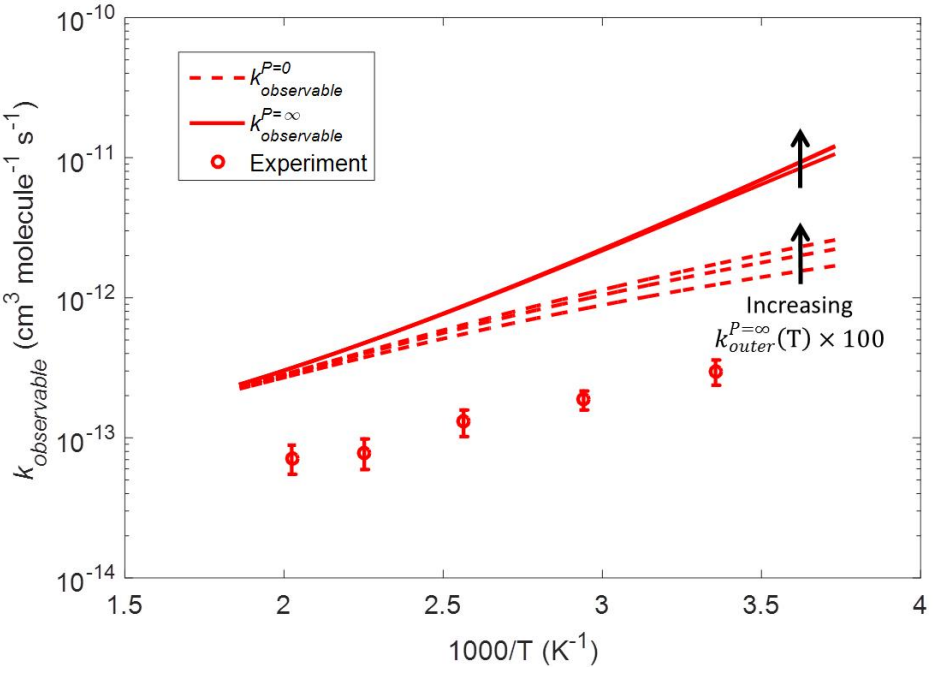

(b)

Figure S6. Predicted T-dependence of $k^{P=0}_{observable}$ and $k^{P=\infty}_{observable}$ over a range of $k^{P=\infty}_{outer}$ for (a) CH_2OO + CH_3CHO and (b) CH_2OO + CH_3COCH_3

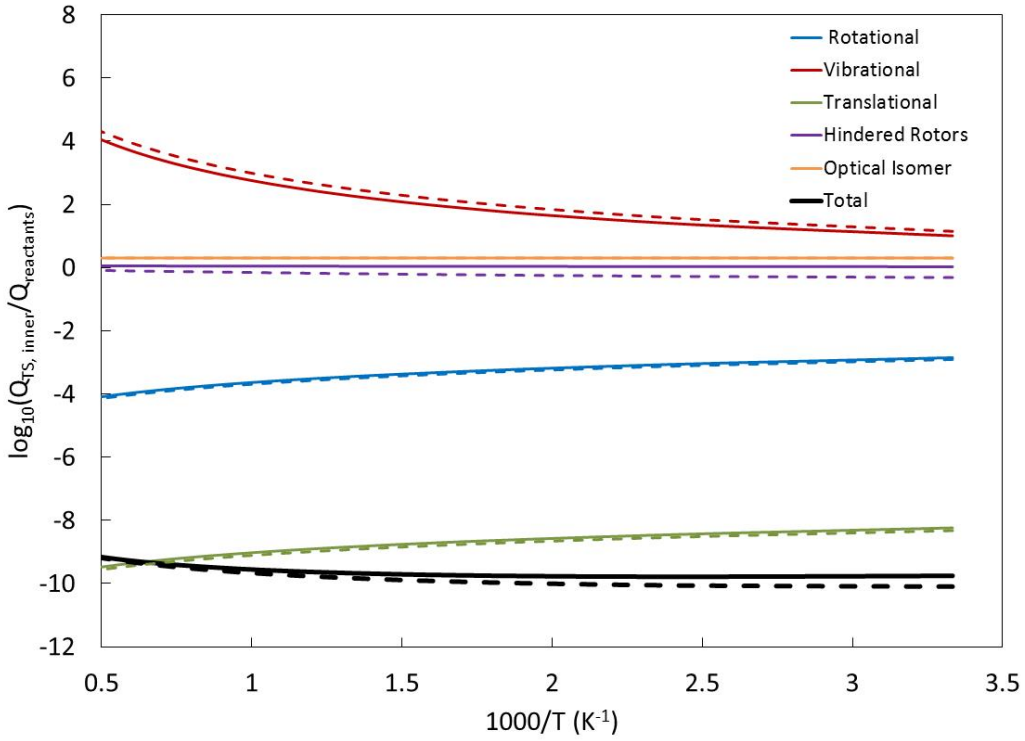

Figure S7. Different contributions to the ratio $Q_{TS,inner}/Q_{reactants}$ in the TST expression for the high-P limit *k*, demonstrating the dominance of the vibrational term at higher temperatures. Solid lines are for CH_2OO + CH_3CHO and dashed lines are for CH_2OO + CH_3COCH_3.

Comparison of Predictions with HCHO Yield Measurements of Stone et al.

Using HCHO laser-induced fluorescence (LIF), Stone et al. quantified yields of HCHO from CH_2OO + CH_3CHO at 295 K in 25 to 300 Torr of mostly N_2 bath gas.[11] They observed that the yield decreased significantly with increasing pressure and by fitting their data to a Stern-Volmer equation they were able to estimate an HCHO yield of 88% at 4 Torr and 4% at 730 Torr (in N_2). At first glance, these measurements seem to be inconsistent with our own predictions of the CH_2OO + CH_3CHO product distribution, wherein the low-pressure HCHO yield at room temperature is ~25%, and the remaining ~75% is attributable to HCOOH + CH_3CHO (see Fig. 10 of main text and Fig. S8a below). However, this discrepancy can be explained by uncertainties in both the measurements of Stone et al. and our predictions.

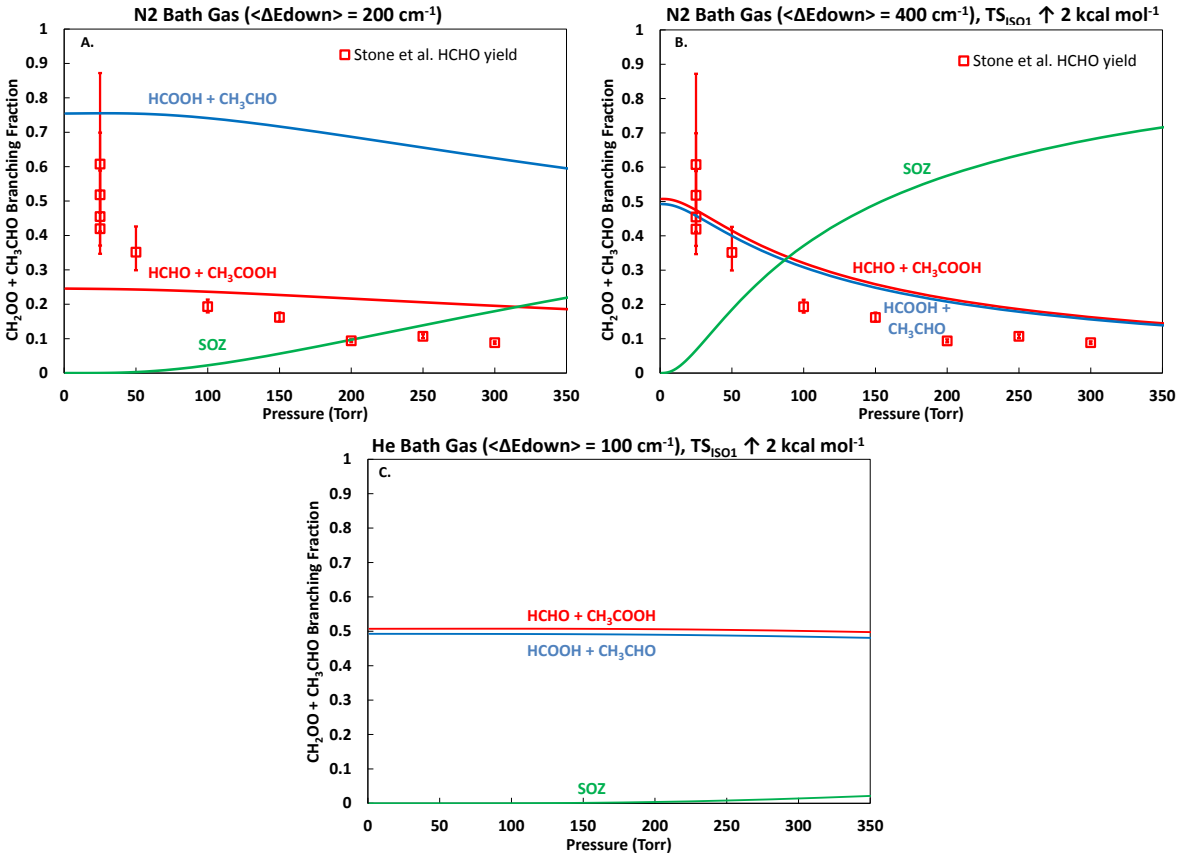

Figure S8. Comparison between HCHO yield measured by Stone et al.[11], and our predictions using the methodology of Jalan et al.[10] with the modifications indicated.

First, in order to obtain the estimates of the HCHO yield above, Stone et al. forced the intercept of their Stern-Volmer plot to equal 1.0, which is tantamount to assuming that in the low-P limit, HCHO is the only product. The authors report that without this assumption, the intercept of the fit is 1.19 ± 0.39, which corresponds to low-pressure HCHO yields in the range of 63-100%. The remainder of the yield can be attributed to the HCOOH + CH_3CHO

product channel, consistent with our predictions and also with the PI TOF-MS measurements of Taatjes et al., where HCHO, CH_3COOH and HCOOH were all observed as products of CH_2OO + CH_3CHO in 4 Torr He.[2]

Second, as demonstrated by Jalan et al., the predicted product branching is quite sensitive to certain transition state energies, as well as the energy transfer model.[10] It was previously shown that the yield of HCHO versus HCOOH is predominantly controlled by the energies of the transition states labelled TS_{ISO1} and TS_{ISO2}, which are only separated by 1.6 kcal mol^{-1}. For the purpose of quantitative comparison with Stone et al., we have increased TS_{ISO1} until our low-pressure predictions are in good agreement with their 25 Torr measurements (Fig. S8b). An increase of 2 kcal mol^{-1} was necessary, which is reasonable given the level of theory used (RCCSD(T)-F12a/VTZ-F12//B3LYP/MG3S) and also considering that in reality it is the combined uncertainty of TS_{ISO1} and TS_{ISO2} (as well as TS_{D3} possibly) that leads to the observed discrepancy.

In order to capture the pressure dependence of the yield measured by Stone et al., we also increased $< \Delta E_{down} >$ for an N_2 bath gas from 200 cm^{-1} to 400 cm^{-1} (Fig. S8b). Although Jalan et al. used the former value for their original predictions in an N_2 bath gas (taken from an *ab initio* study of monomethylhydrazine, CH_3NHNH_2, decomposition in N_2[12]), the latter value also has precedence in the literature (toluene in N_2, for example[13]). Even with this large adjustment, however, our predicted decrease in HCHO yield with pressure is not as steep as Stone et al.'s measurement. This might be explained by underestimated uncertainty in the higher-pressure measurements of Stone et al., where the presence of CH_2IOO complicates their analysis. Furthermore, the scatter in the data at the lowest pressure (25 Torr) suggests that the real uncertainty in the yield at a given pressure is larger than what is indicated by the error bars on an individual measurement.

Finally, as a consistency check, we calculated the product branching at our experimental conditions (4-100 Torr He bath gas) using the modified PES (TS_{ISO1} increased by 2 kcal mol^{-1}). Fig. S8c shows that even up to 100 Torr the branching to SOZ is negligible, consistent with the lack of SOZ observed by either us or Taatjes et al. at these conditions.

References

1.CRC Handbook of Chemistry and Physics. In Physical Constants of Organic Compounds [Online] 89 ed.; Lide, D. R., Ed. CRC Press/Taylor and Francis: Boca Raton, FL, 2009.

2. C. A. Taatjes, O. Welz, A. J. Eskola, J. D. Savee, D. L. Osborn,E. P. F. Lee, J. M. Dyke, D. W. K. Mok, D. E. Shallcross and C. J. Percival, *Phys. Chem. Chem. Phys.*, 2012, **14**, 10391–10400.

3. S. L. Baughcum and S. R. Leone, *J. Chem. Phys.* 1980, **72** (12), 6531-6545.

4. Z. J. Buras, R. M. I. Elsamra, A. Jalan, J. E. Middaugh, W. H. Green, *J. Phys. Chem. A*, 2014, **118**, 1997- 2006.

5. A. J. Eskola, D. Wojcik-Pastuszka, E. Ratajczak, R. S. Timonen, *Phys. Chem. Chem. Phys.* 2006, ***8***, 1416-1424.

6. L. Vereecken, H. Harder, A. Novelli, *Phys. Chem. Chem. Phys.* 2014, 4039-4049.

7. Z. J. Buras, R. M. I. Elsamra, W. H. Green, *J. Phys. Chem. Lett*. 2014, **5**, 2224-2228.

8. W.-L. Ting, C-H. Chang, Y.-F. Lee, H. Matsui, Y.-P. Lee, J. J.-M. Lee, *J. Chem. Phys.* 2014, **141**.

9. R. Chhantyal-Pun, A. Davey, D. E. Shallcross, C. J. Percival, A. J. Orr-Ewing, *Phys. Chem. Chen. Phys.* 2015, **17**, 3617-3626.

10. A. Jalan, J. W. Allen, W. H. Green, *Phys. Chem. Chem. Phys.*, 2013, **15**, 16841- 16852.

11. D. Stone, M. Blitz, L. Daubney, N. U. M. Howes, P. Seakins, *Phys. Chem. Chem. Phys.* 2014, **16**, 1139-1149.

12. P. Zhang, S. J. Klippenstein, H. Sun, C. K. Law, *Proc. Comb. Inst.* 2011, **33**, 425-532.

13. J. A. Miller and S.J. Klippenstein, *J. Phys. Chem. A.* 2003, **107**, 7783-7799.